Journal of Alloys and Compounds 495 (2010) 39–44

Contents lists available at ScienceDirect

Journal of Alloys and Compounds

journal homepage: www.elsevier.com/locate/jallcom

Phase relations of the Eu–Zn–Al system at 400 °C from 0 to 33.3 at.% Eu

Yu. Verbovytskyy[a,*], L.C. Alves[b], A.P. Gonçalves[a]

[a] Departamento de Química, Instituto Tecnológico e Nuclear/CFMC-UL, Estrada Nacional 10, P-2686-953 Sacavém Codex, Portugal
[b] Unidade de Física e Aceleradores, Instituto Tecnológico e Nuclear/CFN-UL, P-2686-953 Sacavém Codex, Portugal

ARTICLE INFO

Article history:
Received 10 December 2009
Received in revised form 18 January 2010
Accepted 21 January 2010
Available online 1 February 2010

Keywords:
Intermetallics
Phase diagrams
X-ray diffraction

ABSTRACT

The phase relations in the Eu–Zn–Al ternary system have been established at 400 °C for the partial isothermal section in the 0–33.3 at.% europium concentration range, by means of X-ray powder diffraction (XRPD), optical microscopy (OM) and particle induced X-ray emission microscopy (μPIXE). The existence of three new ternary compounds was found and their crystal structures were assigned: $Eu_2Zn_{13.9-14.3}Al_{3.1-2.7}$ (Th_2Zn_{17}-type), $Eu_3Zn_{18}Al_4$ (Ce_3Zn_{22}-type) and $EuZn_{1-2}Al_{3-2}$ ($BaAl_4$-type). All binary compounds from the Eu–Al and Eu–Zn system reveal homogeneity ranges by Zn/Al substitutions.

1. Introduction

Numerous of rare earth and transition metal alloys possess valuable magnetic and electrical properties. Some of them are interesting because of their unusual behaviour, exhibiting mixed valence, heavy fermion and Kondo effects. They, as the new technologically important materials, also provide many potential or already realized applications in industry. So, there is an increasing interest for the investigations of the phase diagrams, composition and crystal structure of the ternary compounds in the rare earth, *d*- and *p*-metals systems. This work is continuation of a such systematic research and presents results on the phase relations in the ternary Eu–Zn–Al system at 400 °C obtained from X-ray powder diffraction (XRPD), optical microscopy (OM) and particle induced X-ray emission microscopy (μPIXE) data.

Among the R–Zn–Al systems, the isothermal sections were constructed only for the Ce–Zn–Al system at 320 °C, based on experimental data [1], and for the Y–Zn–Al system at 300 °C and 500 °C, based on thermodynamic calculations [2]. In the other systems only certain $R_xZn_yAl_z$ compositions were investigated [3–12].

Seventeen ternary phases from the Yb–Zn–Al system have been reported [3–9] and their crystal structures were determined: $YbZn_{0.8-1}Al_{0.2-0}$ (CsCl-type), $YbZn_{1.7-2}Al_{0.3-0}$ ($CeCu_2$-type), $YbZn_{1.46-1.67}Al_{0.54-0.33}$ ($MgZn_2$-type), $YbZn_{0.99-1.32}Al_{1.01-0.68}$ ($MgNi_2$-type), $YbZn_{0-0.88}Al_{2-1.12}$ ($MgCu_2$-type), $YbZn_{2.12-2.6}Al_{0.88-0.4}$ ($CeNi_3$-type), $YbZn_{0.92-1.08}Al_{2.08-1.92}$ ($PuNi_3$-type), $Yb_3Zn_{4-6.16}Al_{7-4.84}$ and $Yb_3Zn_{10.6-11}Al_{0.4-0}$ (La_3Al_{11}-type), $YbZn_{4.44-5.86}Al_{0.30-0}$ (related to YCd_6-type), $YbZn_{1.65}Al_{2.35}$ ($BaAl_4$-type), $Yb_8Zn_{41.4-48.5}Al_{24.6-17.5}$ ($Yb_6Cu_{17}Al_{49}$-type), $Yb_2Zn_{15.61}Al_{0.71}$ (derived from U_2Zn_{17}-type), $Yb_{6.4}Zn_{46.8}Al_{3.4}$ (own type), $YbZn_{9.21}Al_{1.29}$ (derived from $SmZm_{11}$-type), $Yb_3Zn_{17.7}Al_{4.3}$ (Ce_3Zn_{22}-type) and $YbZn_{8.5}Al_{2.5}$ ($BaHg_{11}$-type).

Iiandelli [10] investigated alloys from the RZn_2–RAl_2 cross-section for R = Ce, Sm, Gd, Er. Three different structures were found for the intermediate phases: $CeCu_2$-type ($CeZn_{1-2}Al_{1-0}$, $SmZn_{1-2}Al_{1-0}$, $GdZn_{1.1-2}Al_{0.9-0}$ and $ErZn_{1.4-2}Al_{0.6-0}$), $CaIn_2$-type ($SmZn_{0.8-0.9}Al_{1.2-1.1}$, $GdZn_{0.7-1}Al_{1.3-1}$ and $ErZn_{0.7-1.3}Al_{1.3-0.7}$) and $MgCu_2$-type ($CeZn_{0-0.6}Al_{2-1.4}$, $SmZn_{0-0.2}Al_{2-1.8}$ and $ErZn_{0-0.1}Al_{2-1.9}$). Information on existence of the RZn_2Al_2 (R = La, Ce, Pr, Sm) compounds with $CeAl_2Ga_2$-type were presented in [2,11 and reference herein]. The discovery of the new $HoZn_5Al_3$-type and their representatives in some other R–Zn–Al systems ($YZn_{5.52}Al_{2.48}$, $DyZn_{4.96}Al_{3.04}$, $ErZn_{5.37}Al_{2.63}$, $TmZn_{5.64}Al_{2.36}$ and $LuZn_{5.58}Al_{2.42}$) were given in [12].

2. Literature data

A brief summary of the literature data focusing on the phase equilibrium of the binary Eu–Zn–Al subsystems is presented below. A list of the solid phases formed in the three binary systems involved is given in Table 1.

The Eu–Al phase diagram has been presented by Okamoto [13]. Three binary compounds exist in this system: $EuAl_4$ ($BaAl_4$-type), $EuAl_2$ ($MgCu_2$-type) and EuAl (own type) [14–16]. The $EuAl_2$ melts congruently at ~1300 °C. The other two compounds, namely, $EuAl_4$ and EuAl, are obtained by the peritectic reactions $L + EuAl_2 = EuAl_4$ (~800 °C) and $L + EuAl_2 = EuAl$ (~950 °C), respectively.

* Corresponding author. Tel.: +351 219946100; fax: +351 219946185.
E-mail address: yuryvv@bigmir.net (Yu. Verbovytskyy).

0925-8388/$ – see front matter © 2010 Elsevier B.V. All rights reserved.
doi:10.1016/j.jallcom.2010.01.108

Table 1
Literature data on binary compounds the Eu–Zn–Al system.

Phase	Transformation Temperature (°C)[a]	Structure type	Space group	Lattice parameters (Å)			Reference
				a	*b*	*c*	
$EuAl_4$	800, p	$BaAl_4$	*I*4/*mmm*	4.398	–	11.170	[14]
$EuAl_2$	1300, mp	$MgCu_2$	*Fd*$\bar{3}$*m*	8.1262	–	–	[15]
EuAl	950, p	Own	*Pnnm*	5.806	9.652	10.088	[16]
$EuZn_{13}$	?	$NaZn_{13}$	*Fm*$\bar{3}$*c*	12.216	–	–	[18]
$EuZn_{11}$	?	$BaCd_{11}$	$I4_1/amd$	10.719	–	6.874	[18]
$EuZn_5$	?	$CaCu_5$	*P*6/*mmm*	5.473	–	4.286	[19]
$EuZn_2$	740, mp	$CeCu_2$	*Imma*	4.728	7.650	7.655	[20]
EuZn	660, mp	CsCl	*Pm*$\bar{3}$*m*	3.808	–	–	[21]
Zn_3Al_2	?	Cu	*Fm*$\bar{3}$*m*	–	–	–	[22]
$ZnAl_2$	?	Own	*P*$\bar{3}$*m*	2.86	–	6.99	[25]
$Zn_{0.29}Al_{0.71}$	?	Own	*R*$\bar{3}$*m*	2.852	–	6.785	[26]

[a] mp: melting point; p: peritectic reaction.

The total binary Eu–Zn system was not yet constructed. A partial phase diagram was presented by Massalski [17]. The existence of five compounds has been established [18–20]: $EuZn_{13}$ ($NaZn_{13}$-type), $EuZn_{11}$ ($BaCd_{11}$-type), $EuZn_5$ ($CaCu_5$-type), $EuZn_2$ ($CeCu_2$-type), EuZn (CsCl-type). The EuZn and $EuZn_2$ melt congruently at 660 and 740 °C, respectively. The transformations temperatures of the other compounds are still unknown.

The binary Zn–Al is the most explored system. In the earlier publications on this phase diagram [21,22] it was indicated the existence of an intermediate phase with the Zn_3Al_2 composition. Further investigations [23,24] have shown that Zn_3Al_2 is not an individual phase, but it is a part of an extended solid solution of zinc in aluminium: $Zn_{67}Al_{33}$–Al_{100}. Later works [25,26] indicated the existence of two binary, probably metastable, phases, $ZnAl_2$ and $Zn_{0.29}Al_{0.71}$, with own structure types. One monotectoid transformation, with the ~58.5Zn:41.5Ga composition, is observed in this system at 277 °C. No significant changes were recently made on the Zn–Al phase diagram [27].

3. Experimental details

A total of 70 binary and ternary samples have been prepared and analysed in the present work, their compositions being shown in Fig. 1. Metals with nominal purities >99.95 wt.% (europium ingots, zinc tear drops and aluminium pieces) were used as starting materials. Each sample was synthesized by direct melting of the elements inside quartz ampoules under vacuum (10^{-5} Torr). The reactions were first performed at 950 °C, the ampoules being hold at that temperature for 1 h, followed by their cooling in air. The obtained products, with metallic-like lustres, were studied by X-ray powder diffraction technique. No reaction with the quartz ampoules was observed. Finally, fragments of the as-prepared ingots were sealed in evacuated quartz tubes and annealed at 400 °C for 20 days, inside a vertical oven. After the heat treatments, the samples were quenched by submerging the quartz tubes in cold water and analysed.

A PANalytical X'Pert Pro diffractometer (Cu Kα-radiation) was used for the X-ray phase and structural analyses of the powdered polycrystalline samples. The scans were taken in the $\theta/2\theta$ mode with the following parameters: 2θ region, 15–120°; step scan, 0.03°; counting time per step, 10–20 s. Theoretical powder patterns were calculated with the help of the PowderCell program [28] and used for the identification of the phases. The lattice parameters were obtained by least-squares fitting using the Latcon program [29]. The FullProf [30] program was used for single and multi phase Rietveld fittings. Fig. 2 illustrates X-ray diffractions patterns of selected Eu–Zn–Al alloys.

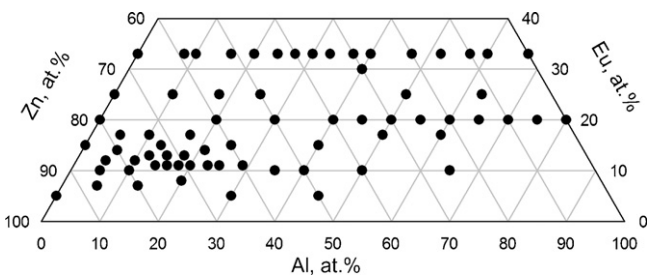

Fig. 1. Compositions of the Eu–Zn–Al samples.

The microstructure of the samples was first studied, on polished and etched surfaces, by using an optical microscope Olympus OM150 (Fig. 3).

Selected samples were then analysed using the Oxford Microbeams type ITN nuclear microprobe that is able to focus down to 3 μm × 4 μm a 1 MeV proton beam generated by a 2.5 MV Van de Graaff accelerator. The focused proton beam was raster scanned over the samples and the produced X-rays (μPIXE technique) collected with an 80 mm^2 of 145 eV resolution Si(Li) detector positioned at 45° to the beam direction. A 200 mm^2 Si particle detector positioned at 40° to the beam direction was also used to detect backscattered particles (RBS technique) and was mainly employed for beam charge normalization. Microprobe control and data handling was accomplished through OMDAQ [31] computer code, that also allowed obtaining elemental distribution maps. The proton beam current was kept between 100 and 200 pA.

A large beam scan (maximum of 3730 μm × 3730 μm for 1 MeV proton beam) was carried out in order to center the sample of interest and further zooming performed down to an area of 370 μm × 370 μm. Point analysis was then performed in order to obtain quantitative results, using the GUPIX code [32] included in the DAN32 [33] software package.

Usually, a 50 μm Mylar filter protects the Si(Li) detector, preventing the backscattered protons to enter the detector and progressively damage it. However this same filter strongly attenuates the Al K X-rays, leading to a large error in the quantitative analysis. For these reasons the Mylar filter was removed and the proton beam energy was reduced to 1 MeV.

Calibration parameters for performing quantitative analysis were ascertained through the analysis of the Al_2SiO_5 standard and as-prepared $EuAl_4$ and $EuZn_{11}$ samples.

4. Results and discussion

Samples from the aluminium-rich region usually contain the binary $EuAl_4$ and $EuAl_2$ compounds, in agreement with the literature data, which indicate that they are stable at 400 °C. The existence of other four binary phases from the Eu–Zn system ($EuZn_{13}$, $EuZn_{11}$, $EuZn_5$ and $EuZn_2$), also previously reported to be stable at that temperature, were confirmed, their crystallographic analysis agreeing with the reported data.

The binary $EuZn_{13}$ compound dissolves up to about 8 at.% Al in annealed and in as-prepared samples. Only 2 at.% Al substitutes zinc in the binary $EuZn_{11}$ compound. Solubility of aluminium in $EuZn_5$ extends up to the $EuZn_{4.4}Al_{0.6}$ (~10 at.% Al) composition in annealed and to the $EuZn_4Al$ (~17 at.% Al) in as-prepared samples.

In order to study the solid solution ranges of the ternary $EuZn_{2-x}Al_x$ and $EuZn_xAl_{2-x}$ phases, 16 Eu–Zn–Al alloy samples with 33.3 at.% europium and different Zn:Al ratios have been examined. However, X-ray phase analyses of as-prepared and annealed samples indicated the formation of europium oxides and hydroxides. This leads to a decrease of europium content, which results in a deviation from the 33.3 at.% europium line and therefore to the formation of multiphasic samples. Limit compositions of the solid solutions based on binary $EuZn_2$ and $EuAl_2$ compounds have been obtained from the Rietveld refinements, which dissolves about 25 at.% aluminium and 15 at.% zinc, respectively.

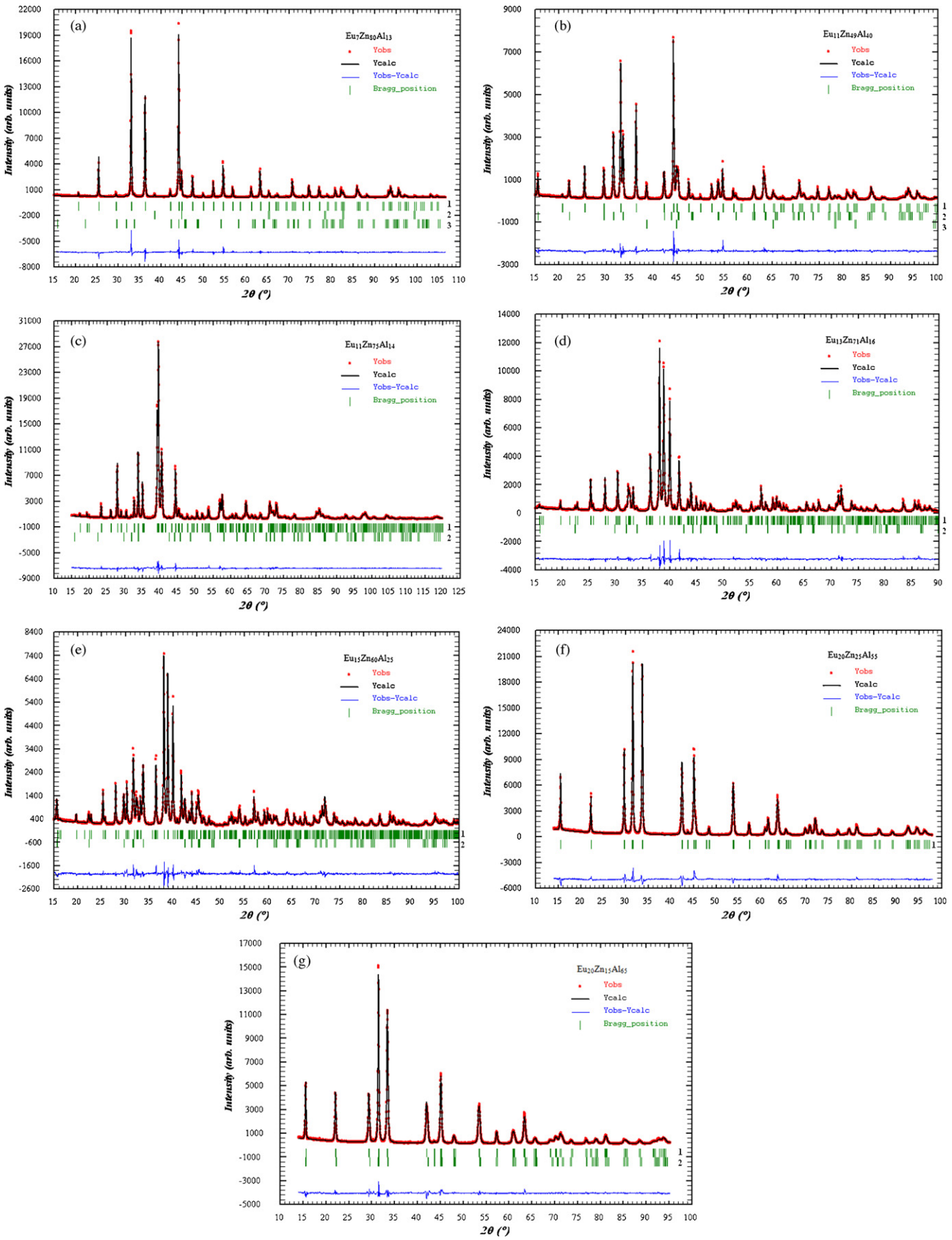

Fig. 2. X-ray diffraction patterns of some Eu–Zn–Al alloys: (a) $Eu_7Zn_{80}Al_{13}$ (1, $EuZn_{13-x}Al_x$; 2, $Al_{1-x}Zn_x$; 3, Zn); (b) $Eu_{11}Zn_{49}Al_{40}$ (1, $EuZn_{13-x}Al_x$; 2, $EuZn_xAl_{4-x}$; 3, $Al_{1-x}Zn_x$); (c) $Eu_{11}Zn_{75}Al_{14}$ (1, $Eu_2Zn_{14.3}Al_{2.7}$; 2, $EuZn_2Al_2$); (d) $Eu_{13}Zn_{71}Al_{16}$ (1, $Eu_3Zn_{18}Al_4$; 2, $EuZn_2Al_2$); (e) $Eu_{15}Zn_{60}Al_{25}$ (1, $Eu_3Zn_{18}Al_4$; 2, $EuZn_2Al_2$); (f) $Eu_{20}Zn_{25}Al_{55}$ (1, $EuZn_{1.25}Al_{2.75}$); (g) $Eu_{20}Zn_{15}Al_{65}$ (1, $EuZn_xAl_{4-x}$; 2, $EuZnAl_3$).

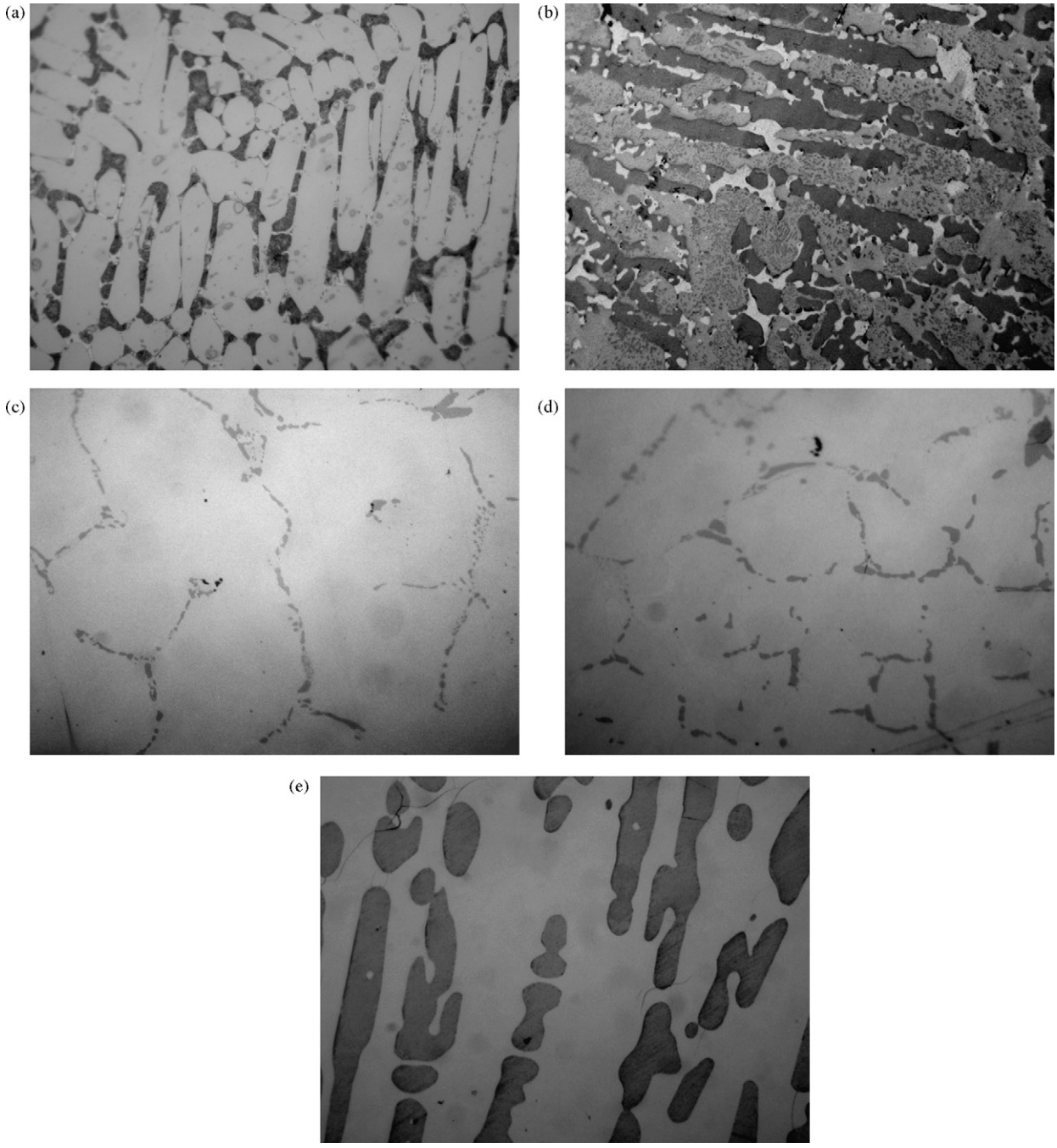

Fig. 3. Microphotographs of some Eu–Zn–Al alloys: (a) $Eu_7Zn_{80}Al_{13}$ (500×); (b) $Eu_{11}Zn_{49}Al_{40}$ (200×); (c) $Eu_{11}Zn_{75}Al_{14}$ (500×); (d) $Eu_{13}Zn_{71}Al_{16}$ (500×); (e) $Eu_{15}Zn_{60}Al_{25}$ (500×).

Table 2
New ternary phases in the Eu–Zn–Al systems.

Phase	Structure type	Space group	Lattice parameters (Å, Å^3)			Remark
			a	*c*	*V*	
$Eu_2Zn_{17-x}Al_x$ (τ_1)	Th_2Zn_{17}	$R\bar{3}m$	9.1802(2)	13.3722(3)	975.97(4)	$x = 2.7$
			9.1894(2)	13.3704(3)	977.80(4)	$x = 3.1$
$Eu_3Zn_{22-x}Al_x$ (τ_2)	Ce_3Zn_{22}	$I4_1/amd$	9.0168(2)	21.5989(5)	1756.06(6)	$x = 4$
$EuZn_{4-x}Al_x$ (τ_3)	$BaAl_4$	$I4/mmm$	4.2518(2)	11.3124(7)	204.50(2)	$x = 2$
			4.2545(3)	11.3510(9)	205.46(3)	$x = 2.5$
			4.2611(1)	11.4005(4)	207.00(1)	$x = 2.75$
			4.2817(2)	11.3946(7)	208.89(1)	$x = 3$

In the binary $EuAl_4$ compound zinc solubility reached the $EuZn_{0.25}Al_{3.75}$ composition.

Figs. 2a and 3a, respectively, presents X-ray diffraction pattern and microstructure of the $Eu_7Zn_{80}Al_{13}$ alloy. It consists of the ternary $EuZn_{13-x}Al_x$ ($NaZn_{13}$-type) phase and two solid solutions from binary Zn–Al system based on pure metals, $Al_{1-x}Zn_x$ (Cu-type) and Zn (Mg-type), respectively. According to the microprobe analyses of this sample, average compositions of the main grey and intergranular dark phases were determined as $Eu_{6.7}Zn_{84.9}Al_{8.4}$ and $Eu_{1.6}Zn_{58.9}Al_{39.5}$, respectively. These results are in agreement with the XRD data and indicate that the phase with the $NaZn_{13}$-type structure has the $Eu_{6.7}Zn_{84.9}Al_{8.4}$ composition and that the intergranular phase is $Al_{1-x}Zn_x$.

X-ray diffraction pattern and microstructure of the $Eu_{11}Zn_{49}Al_{40}$ alloy, respectively, are displayed in Figs. 2b and 3b. X-ray phase analysis of the above cited alloy indicated the existence of three phases: $EuZn_{13-x}Al_x$ ($NaZn_{13}$-type), $EuAl_4$ ($BaAl_4$-type) and $Al_{1-x}Zn_x$ (Cu-type).

During the study of the as-prepared and annealed Zn-rich samples we found two new compounds, namely, $Eu_2Zn_{13.9-14.3}Al_{3.1-2.7}$ (τ_1) and $Eu_3Zn_{18}Al_4$ (τ_2), with small homogeneity ranges.

X-ray diffraction data for the first one, $\sim Eu_2Zn_{14}Al_3$ (τ_1), was well indexed by an hexagonal unit cell with lattice parameters $a \sim 9.18$ Å and $c \sim 13.37$ Å. Characteristic intensity of the peaks and composition indicated on the Th_2Zn_{17} structure type (space group $R\bar{3}m$) for the above mentioned compound. Crystal structure refinement for the $Eu_{11}Zn_{75}Al_{14}$ alloy using Rietveld method confirmed this hypothesis (Fig. 2c), also showing small amounts of a second phase with the $BaAl_4$-type structure. The cell parameters obtained during the XRD data fitting of annealed samples are shown in Table 2. Microstructure of the $Eu_{11}Zn_{75}Al_{14}$ alloy is plotted in Fig. 3c. Microprobe analyses of this sample agree with XRD results, revealing the formation of the $Eu_2Zn_{17-x}Al_x$ compound (grey phase), with $\sim Eu_{10.2}Zn_{78.4}Al_{11.4}$ average composition, together with dark dots, which correspond to the $\sim EuZn_2Al_2$ phase.

Another Zn-rich compound (τ_2), with the $\sim Eu_3Zn_{18}Al_4$ composition, was found on the cross-section with 12 at.% Eu. X-ray diffraction pattern of alloy close to this composition indicated a more complex structure, with comparison of XRD for $Eu_2Zn_{17-x}Al_x$ phase. Having generated for different models for well-known structures of binary R–Zn and ternary R–Zn–X compounds, our attention was stopped on the Ce_3Zn_{22}-type structure (space group $I4_1/amd$). X-ray diffraction data for the $Eu_{13}Zn_{71}Al_{16}$ phase was successfully fitted considering this structure type (Fig. 2d). Calculated lattice parameters of this intermetallic compound are presented in Table 2. Fig. 3d shows the microstructure of the $Eu_{13}Zn_{71}Al_{16}$ alloy. This sample consists of two phases: $Eu_3Zn_{18}Al_4$ (main grey phase, Ce_3Zn_{22}-type) and $EuZn_2Al_2$ (secondary dark phase, $BaAl_4$-type). Average composition of the main phase, $Eu_{11.9}Zn_{70.2}Al_{17.9}$, was obtained from PIXE microprobe analyses and it is with good agreement with XRD data.

X-ray diffraction pattern and microstructure of the $Eu_{15}Zn_{60}Al_{25}$ alloy are shown in Figs. 2e and 3e show, respectively. According to the XRD data, this sample consists of two phases: $Eu_3Zn_{18}Al_4$, with Ce_3Zn_{22}-type, and $EuZn_2Al_2$ with $BaAl_4$-type structures.

In the as-prepared and annealed alloys with compositions along the cross-section with 20 at.% europium a new ternary $EuZn_{4-x}Al_x$ compound (τ_3) was found. This new intermetallic phase has an extended homogeneity range including the composition $EuZn_2Al_2$ and $EuZnAl_3$, and crystallizes with $BaAl_4$ structure type (space group $I4/mmm$). X-ray diffraction pattern of the annealed $Eu_{20}Zn_{25}Al_{55}$ alloy is presented in Fig. 2f. Average composition, $Eu_{19.0}Zn_{25.9}Al_{55.1}$, obtained from PIXE analyses for this sample, is close to the nominal one. The increase of the aluminium content results on an increment of the lattice parameters (Table 2), in agreement with the bigger atomic dimensions of aluminium with respect to zinc.

It should be noted that the binary $EuAl_4$ compound also belongs to the $BaAl_4$-type and is in equilibrium with the ternary $EuZn_{4-x}Al_x$ compound. X-ray diffraction pattern of the annealed $Eu_{20}Zn_{15}Al_{65}$ alloy (Fig. 2g) consists of these two phases with the similar structures. The nature of the coexisting phases with $BaAl_4$ is still unknown. Most probably, by replacing a certain amount of aluminium for zinc in the binary $EuAl_4$ compound leads to a change of the VEC (valence electron concentration) and to the stabilization of the new ternary compound with the same structure.

The crystallographic data on the new ternary Eu–Zn–Al phases are collected in Table 2. Herein, we present only the lattice parameters of these compounds. Single crystal studies, accurate crystal structure determination, magnetic and transport physical properties of ternary Eu–Zn–Al phases will be published in a further paper.

The isothermal section of the Eu–Zn–Al phase diagram (0–33.3 at.% Eu) at 400 °C, constructed from the X-ray powder diffraction and PIXE experimental results, is shown in Fig. 4. In this partial isothermal section 13 ternary phase fields have been identified, those are listed below in order of increasing of aluminium contents:

(1) $Zn + L + EuZn_{13-x}Al_x$;
(2) $EuZn_{13-x}Al_x + EuZn_{11-x}Al_x + \tau_1$;
(3) $EuZn_{11-x}Al_x + EuZn_{5-x}Al_x + \tau_1$;
(4) $L + EuZn_{13-x}Al_x + Al_{1-x}Zn_x$;
(5) $EuZn_{13-x}Al_x + Al_{1-x}Zn_x + EuZn_xAl_{4-x}$;
(6) $EuZn_{13-x}Al_x + \tau_1 + EuZn_xAl_{4-x}$;
(7) $\tau_1 + \tau_2 + EuZn_{5-x}Al_x$;
(8) $\tau_1 + \tau_2 + \tau_3$;
(9) $\tau_2 + EuZn_{5-x}Al_x + \tau_3$;
(10) $\tau_2 + EuZn_{5-x}Al_x + EuZn_{2-x}Al_x$;
(11) $\tau_1 + \tau_3 + EuZn_xAl_{4-x}$;
(12) $\tau_3 + EuZn_{2-x}Al_x + EuZn_xAl_{2-x}$;
(13) $\tau_3 + EuZn_xAl_{4-x} + EuZn_xAl_{2-x}$.

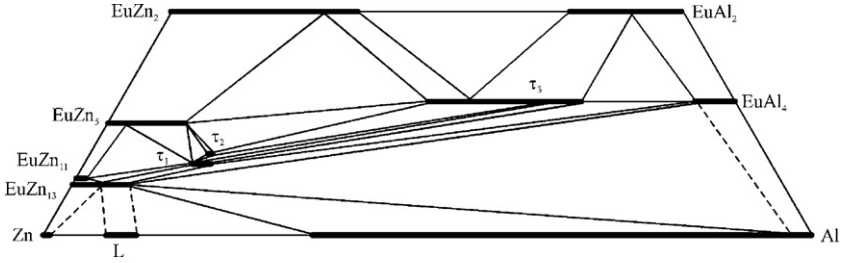

Fig. 4. Isothermal section of the ternary Eu–Zn–Al phase diagram at 400 °C with 0–33.3 at.%. (τ_1) $Eu_2Zn_{13.9-14.3}Al_{3.1-2.7}$, ($\tau_2$) $Eu_3Zn_{18}Al_4$, and (τ_3) $EuZn_{1-2}Al_{3-2}$.

Table 3
Summarized data on interaction among the components in the Eu–M–Al system.

IIIA	IVA	VA	VIA	VIIA		VIIIA		IB	IIB
Sc	Ti	V	Cr	Mn	Fe	Co	Ni	Cu	Zn
–	1	1	2	3 △	2	–	1	6 ▲	3 △[a]
Y	Zr	Nb	Mo	Tc	Ru	Rh	Pd	Ag	Cd
–	–	1	1	–	–	–	–	2	–
La	Hf	Ta	W	Re	Os	Ir	Pt	Au	Hg
–	–	1	1	–	–	–	–	1	–

▲ or △ – isothermal section built in the whole concentration region or in part of it, respectively; (*N*) number of ternary phases; (–) no data available or ternary phases did not find yet.

[a] This work.

Summarized data on the interaction among the components in the europium–*d*-metal–aluminium systems are shown in Table 3 (the number of ternary phases, N, are presented). According to our best knowledge, the isothermal sections were constructed, in the partial or whole concentration region, only for three systems (including this work on Eu–Zn–Al), and 24 ternary compounds were found [34–37].

The most explored system, Eu–Cu–Al, is characterised by the existence of five ternary compounds and one phase with an extended homogeneity range: $EuCu_4Al_8$ ($ThMn_{12}$-type), $EuCu_2Al_3$ ($PrNi_2Al_3$-type), $EuCu_{0.83}Al_{1.27}$ ($CaCu_{0.83}Al_{1.27}$-type), $EuCu_{0.6}Al_{1.4}$ ($MgNi_2$-type), Eu_6CuAl_3 (unknown type) and $EuCu_{6.2-9.1}Al_{6.8-3.9}$ ($NaZn_{13}$-type). Solid solutions are formed on the basis of the binary $EuCu_5$ ($CaCu_5$-type) and $EuAl_4$ ($BaAl_4$-type) compounds and extended up to the $EuCu_{3.2}Al_{1.8}$ and $EuCu_{0.5}Al_{3.5}$ compositions, respectively [36].

The isothermal section of the Eu–Mn–Al system has been investigated at 500 °C across the composition Al–$EuAl_2$–$Mn_{77}Al_{23}$. Three ternary compounds have been identified and their crystal structures were determined: $EuMn_{2.3-3.6}Al_{9.7-8.4}$ ($ThMn_{12}$-type), $Eu_2Mn_5Al_{12}$ ($Eu_2Re_6S_{11}$-type) and $Eu_2Mn_5Al_{12}$ (Th_2Zn_{17}-type) [37].

Alloys from the $EuAl_2$–$LaAl_2$ and $EuAl_2$–YAl_2 cross-sections have also been investigated [38]. Unlimited solid solutions $Eu_{1-x}La_xAl_2$ and $Eu_{1-x}YAl_2$ ($0 \le x \le 1$) with $MgCu_2$ structure type were discovered. No intermediate phases were found.

All the known ternary aluminides, with established crystal structures, belong to 14 structure types: $Eu_2Re_6S_{11}$, $CeCr_2Al_{20}$, $CaCo_2Al_8$, $NaZn_{13}$, $ThMn_{12}$, $BaCd_{11}$, Th_2Zn_{17}, Ce_3Zn_{22}, $PrNi_2Al_3$, $CaCu_5$, $BaAl_4$, ZrNiAl, $MgNi_2$ and $CaCu_{0.83}Al_{1.27}$.

Comparing Eu–Zn–Al system with the others Eu–*d*-metal–aluminium systems, it should be underlined that ternary compounds with $BaAl_4$ and Th_2Zn_{17} structure types have been found also in the early investigated Eu–Au–Al and Eu–Mn–Al systems, respectively. Ternary phases with Ce_3Zn_{22} structure type have been discovered only in the Eu–Zn–Al system.

Taking into account the results obtained in this work and the reported ones on similar ternary systems, we can deduce the character of the interaction among the components of the yet unexplored R–Zn–X (R – rare earth, X – Al, Ga, In) systems: it is expected the existence of new intermetallic compounds and solid solutions, in particular those based on the partial substitution of the Zn and *p*-atoms.

5. Conclusion

The Eu–Zn–Al alloys have been studied by means of X-ray diffraction and μPIXE microscopy was used for characterizing the formed phases. Six compounds belonging to the binary Eu–Zn and Eu–Al systems, and previously reported to be stable at 400 °C, have been observed in the study of the partial isothermal section of the Eu–Zn–Al phase diagram at that temperature. Three new compounds, $Eu_2Zn_{17-x}Al_x$ (Th_2Zn_{17}-type) ($2.7 \le x \le 3.1$), $Eu_3Zn_{22-x}Al_x$ ($x = 4$) (Ce_3Zn_{22}-type) and $EuZn_{4-x}Al_x$ ($2 \le x \le 3$) ($BaAl_4$-type), were also found to exist at 400 °C. The available data on the studied Eu, *d*- and *p*-metals systems point to the possibility of existence of new compounds and extended homogeneity ranges, based on the partial substitution of the *d*- and *p*-atoms, in the yet unexplored Eu–M–X systems.

Acknowledgments

This work was partially supported by FCT, Portugal, under the contract No. PTDC/QUI/65369/2006. The FCT Grant No. SFRH/BPD/34840/2007 for the research work of Y.V. at ITN, Sacavém, Portugal is highly appreciated.

References

[1] A.Z. Ikromov, I.N. Ganiev, A.V. Vakhobov, V.V. Kinzhibalo, Metally 2 (1991) 217–218.
[2] X.J. Liu, M.Z. Wen, C.P. Wang, F.S. Pan, J. Alloys Compd. 452 (2008) 283–290.
[3] B. Stel'makhovych, O. Stel'makhovych, Yu. Kuz'ma, J. Alloys Compd. 397 (2005) 115–119.
[4] M.L. Fornasini, P. Manfrinetti, D. Mazzone, Acta Crystallogr. A 61 (2005) C369.
[5] M.L. Fornasini, P. Manfrinetti, D. Mazzone, J. Solid State Chem. 179 (2006) 2012–2019.
[6] M.L. Fornasini, P. Manfrinetti, D. Mazzone, Intermetallics 15 (2007) 856–861.
[7] M.L. Fornasini, P. Manfrinetti, D. Mazzone, S.K. Dhar, Z. Naturforsch. 63b (2008) 237–243.
[8] D. Mazzone, P. Manfrinetti, M.L. Fornasini, J. Solid State Chem. 182 (2009) 2344–2349.
[9] O. Stel'makhovych, B. Stel'makhovych, Ya. Kalychak, L. Havela, Intermetallics, 2009, doi:10.1016/j.intermet.2009.10.008.
[10] A. Iandelli, J. Less-Common Met. 169 (1991) 187–196.
[11] G. Cordier, E. Czech, H. Schäfer, P. Woll, J. Less-Common Met. 110 (1985) 327–330.
[12] O. Stel'makhovych, Yu. Kuz'ma, Z. Naturforsch. 61 (2006) 779–784.
[13] H. Okamoto, J. Phase Equilibr. 12 (1991) 499–500.
[14] J.H.N. Van Vucht, K.H.J. Buschow, Philip Res. Rep. 19 (1964) 319–322.
[15] R. Harris, R.C. Mansey, G.V. Raynor, J. Less-Common Met. 9 (1965) 270–280.
[16] N.B. Manyako, I.V. Rozhdestvenskaya, O.S. Zarechnyuk, T.I. Yanson, Kristallografiya 30 (1985) 280–282.
[17] T.B. Massalski (Ed.), Binary Alloy Phase Diagrams, vol. 2, second edition, ASM International, Materials Park, OH, 1990, pp. 1688–1689.
[18] A. Iandelli, A. Palenzona, J. Less-Common Met. 12 (1967) 333–343.
[19] Yu.B. Kuz'ma, P.I. Kripyakevich, D.P. Frankevich, Izv. Akad. Nauk SSSR, Neorg. Mater. 1 (1965) 1410–1415.
[20] A. Iandelli, A. Palenzona, G.B. Bonino, Rendiconti 37 (1964) 165–168.
[21] W. Rozenhain, S.L. Archbutt, J. Inst. Met. 6 (1911) 236–258.
[22] D. Hanson, M.L.V. Gayler, J. Inst. Met. 27 (1922) 267–306.
[23] W.L. Fink, L.A. Willey, Trans. AIME 122 (1936) 244–265.
[24] M.L.V. Gayler, E.G. Sutherland, J. Inst. Met. 63 (1938) 123–147.
[25] J. Yan, L. Chunzhi, Y. Minggao, Mater. Lett. 13 (1992) 115–118.
[26] K.K. Rao, H. Herman, E. Parthé, Mater. Sci. Eng. 1 (1966) 162–166.
[27] T.B. Massalski (Ed.), Binary Alloy Phase Diagrams, vol. 1, second edition, ASM International, Materials Park, OH, 1990, pp. 239–241.
[28] G. Nolze, W. Kraus, Powder cell for Windows (Version 2.3), Federal Institute for Materials Research and Testing, Berlin, 1999.
[29] D. Schwarzenbach, Program LATCON, University of Lausanne, Switzerland, 1975.
[30] J. Rodriguez-Carvajal, T. Roisnel, FullProf.98 and WinPLOTR: New Windows 95/NT Applications for Diffraction Commission For Powder Diffraction, International Union for Crystallography, Newsletter No. 20 (May–August) Summer, 1998.
[31] G.W. Grime, M. Dawson, Nucl. Instr. Methods B 104 (1995) 107–113.
[32] J.A. Maxwell, W.J. Teesdale, J.L. Campbell, Nucl. Instr. Methods B 95 (1995) 407–421.
[33] G.W. Grime, Nucl. Instr. Methods B 109–110 (1996) 170–174.
[34] P. Villars (Ed.), Pearson's Handbook, Crystallographic Data for Intermetallic Phases, desk ed., ASM, Materials Park, OH, 1997.
[35] S. Niemann, W. Jeitschko, J. Solid State Chem. 114 (1995) 337–341.
[36] T.I. Yanson, N.B. Manyako, O.S. Zarechnyuk, Izv. Akad. Nauk SSSR, Metally 6 (1992) 175–179.
[37] N.B. Manyako, T.I. Yanson, O.S. Zarechnyuk, Izv. Akad. Nauk SSSR, Metally 5 (1988) 212–215.
[38] A. Iandelli, G.L. Olcese, J. Less-Common Met. 111 (1985) 145–156.